

Article

Not peer-reviewed version

Synthesis and Characterization of Novel Silylated Sm³⁺ and Eu³⁺ Complexes Incorporated into Mesoporous and Dense Silica Nanoparticles

Juliana Jorge , Jaqueline Rodrigues da Silva , Diego Boldo , Kristiane Fanti Del Pino Santos , [Adriana Pereira Duarte](#) , Gustavo Rocha de Castro , [Ricardo Bentes de Azevedo](#) , Ariadna Lafourcade Prada , [Jesús Rafael Rodríguez Amado](#) , Marc Verelst , [Marco Antonio Utrera Martines](#) *

Posted Date: 3 June 2024

doi: 10.20944/preprints202406.0101.v1

Keywords: hybrid materials; mesoporous silica nanoparticles; dense silica nanoparticles; silylated complexes



Preprints.org is a free multidiscipline platform providing preprint service that is dedicated to making early versions of research outputs permanently available and citable. Preprints posted at Preprints.org appear in Web of Science, Crossref, Google Scholar, Scilit, Europe PMC.

Copyright: This is an open access article distributed under the Creative Commons Attribution License which permits unrestricted use, distribution, and reproduction in any medium, provided the original work is properly cited.

Article

Synthesis and Characterization of Novel Silylated Sm³⁺ and Eu³⁺ Complexes Incorporated into Mesoporous and Dense Silica Nanoparticles

Juliana Jorge ¹, Jaqueline Rodrigues da Silva ², Diego Boldo ³, Kristiane Fanti Del Pino Santos ⁴, Adriana Pereira Duarte ⁵, Gustavo Rocha de Castro ⁶, Ricardo Bentes de Azevedo ⁷, Ariadna Lafourcade Prada ⁸, Jesús Rafael Rodríguez Amado ⁹, Marc Verelst ¹⁰ and Marco Antonio Utrera Martines ^{11,*}

¹ Postgraduate Program in Chemistry, Chemistry Institute, Federal University of Mato Grosso do Sul, Campo Grande, MS, Brazil; juliana.jorge@proton.me

² Postgraduate Program in Nanoscience and Nanotechnology, Biological Science Institute, University of Brasilia, Brasilia, DF, Brazil; soljaque@gmail.com

³ Postgraduate Program in Chemistry, Chemistry Institute, Federal University of Mato Grosso do Sul, Campo Grande, MS, Brazil; diegoboldo18@gmail.com

⁴ Postgraduate Program in Chemistry, Chemistry Institute, Federal University of Mato Grosso do Sul, Campo Grande, MS, Brazil; kristianefdp@gmail.com

⁵ Postgraduate Program in Chemistry, Chemistry Institute, Federal University of Mato Grosso do Sul, Campo Grande, MS, Brazil; adriana.duarte@ufms.br

⁶ Postgraduate Program in Environmental biotechnology, Bioscience Institute, Sao Paulo State University, Botucatu, SP, Brazil; gustavo.casgro@unesp.br

⁷ Postgraduate Program in Nanoscience and Nanotechnology, Biological Science Institute, University of Brasilia, Brasilia, DF, Brazil; razevedo@unb.br

⁸ Postgraduate Program in Biotechnology, Faculty of Pharmacy, Food and Nutrition, Federal University of Mato Grosso do Sul, Campo Grande, MS, Brazil; ariadnalafu1977@gmail.com

⁹ Postgraduate Program in Health Sciences. Faculty of Health Sciences. Federal University of Grande Dourados, Dourados, MS, Brazil; jiribilla2009@gmail.com

¹⁰ Postgraduate Program in Materials Science, Center for Materials Elaboration and Structural Studies, University of Toulouse, Toulouse, France; marc.verelst@cemes.fr

¹¹ Postgraduate Program in Chemistry, Chemistry Institute, Federal University of Mato Grosso do Sul, Campo Grande, MS, Brazil; marco.martines@ufms.br

* Correspondence: marco.martines@ufms.br

Abstract: The aim of this manuscript is to synthesize and characterize novel silylated Sm³⁺ and Eu³⁺ complexes and incorporate them into mesoporous silica nanoparticles (MSNs) and dense silica nanoparticles (DSNs). Sm³⁺ and Eu³⁺ ion complexes were chosen for their strong UV-visible emission, deep-red luminescence, and effective interaction with bidentate organic ligands, such as 2-thenoyltrifluoroacetone (tta) and 1,10-phenanthroline (phen). Silylated ligands were employed as coupling agents to form covalent bonds between the complexes and an oxide matrix via a conventional sol-gel process. This approach aims to enhance the thermal stability and photophysical properties of the resulting hybrid material compared to free complexes. The new silylated-bidentate ligand complexes, using tta and phen as organic ligands and 3-chloropropyltriethoxysilane as the silylating agent, were characterized by FTIR, luminescence spectroscopy, and luminescence decay. After incorporation into silica nanoparticles, the hybrid materials were characterized by SEM, TEM, DLS, zeta potential, SAXS, porosity, surface area measurements, luminescence spectroscopy, and MTT assay. The results confirm the successful synthesis of new luminescent silylated complexes with high luminescence intensity and their incorporation into silica nanoparticles.

Keywords: hybrid materials; mesoporous silica nanoparticles; dense silica nanoparticles; silylated complexes

1. Introduction

Silylated lanthanide complexes are complexes of lanthanide ions (elements in the lanthanide series, such as europium or neodymium) with organic silicon compounds called "silylating agents". [1] These complexes are important in various fields, including materials science and biochemistry. In materials science, they are used in displays and optical data storage [2], while in biochemistry they are used as probes for imaging and sensing in living systems. [3]

The specific properties of a silylated lanthanide complex depend on the lanthanide ion and the silylating agent used, silylated complexes of lanthanides can offer several advantages [4], particularly when incorporated into materials for applications such as luminescence, biolabeling, and sensing. Among these advantages it is possible to mention its chemical stability [5], versatile functionalization, enhanced luminescent properties [2], minimized non-radiative decay [6], and customizable surface chemistry.

Despite the advantages, currently, only a small number of studies have reported the synthesis, characterization, and application of silylated complexes. One of these works is the synthesis of a novel betadiketonate ligand with a trimethoxysilyl group, along with its highly luminescent Europium(III) complex, used to create luminescent silica-based hybrids with varied particle types, demonstrating high grafting ratios and potential for numerous applications as reported by Duarte et al. (2012)[5]. Another work is from Aguiar et al. (2016) [4], where three silica gel-based organic-inorganic hybrid materials functionalized with various silanes and EDTA derivatives were synthesized and used to create new luminescent lanthanide complexes, displaying efficient red and green emissions with potential applications as red and green phosphors. Also, Cousiné et al. (2012) [1] reported a series of luminescent Ru(II) complexes with monosilylated-dipyridine ligands were synthesized, fully characterized, and covalently attached to silica nanoparticles, resulting in hybrids with varying luminescence properties and sizes, depending on whether the complexes were incorporated inside the nanoparticles or grafted onto their surface.

Encapsulating complexes in a nanoparticle can provide several advantages, such as: protection of the complex from the surrounding environment, which can improve its stability and shelf-life; targeted delivery of the complex to a specific cell or tissue. [7] The silica nanoparticles can be functionalized with specific molecules or peptides that can bind to receptors on the surface of cells or tissues, allowing for targeted delivery; enhanced fluorescence intensity. [8] Encapsulating the complex in a nanoparticle can increase the fluorescence intensity, making it more sensitive for imaging applications; and, biocompatibility. [7]

It is important to note that the encapsulation process, the size and the shape of the nanoparticles, and the conditions need to be optimized to ensure the stability of the complex and the desired properties of the nanoparticles. [7,9] Also, the biocompatibility and toxicity of the final nanoparticles should be evaluated before using them *in vivo*. [9]

Therefore, silica nanoparticles offer several significant advantages as carriers for biolabeling, theranostics applications, and many others in healthy areas. [10–12] Overall, the unique properties of silica nanoparticles, including their biocompatibility, functionalizability, high loading capacity, and stability, make them highly suitable for advanced biolabeling and theranostics applications, improving the diagnosis and treatment of various diseases. [8] Additionally, nanoparticles are biocompatible and non-toxic, making them suitable for use in biological systems.

Then, the aim of this work is to synthesize new Sm^{3+} and Eu^{3+} silylated complexes to contribute to silylated-lanthanide complexes and hybrids studies, and then to develop new luminescent probes for biolabeling and theranostic applications.

2. Results

2.1. Ligand Silylation and Synthesis of Silylated Sm^{3+} and Eu^{3+} Complexes

FTIR spectra, in the Figure S1, confirms the achievement of the silylated complexes. Band assignment of spectra shows that characteristic bands of ligands (tta and phen) and Si groups of

silylating agent used in the reactions are present, like as 1420 cm^{-1} ($\nu\text{ C=N}$), 1188 cm^{-1} ($\rho\text{ S-O-CH}_3$), 1146 cm^{-1} ($\nu\text{ Si-O}$), 926 cm^{-1} ($\delta\text{ Si-O-C}$), and 717 cm^{-1} ($\delta\text{ CF}_3$). [1,3,5]

Figure 1 presents the excitation and emission spectra for both $\text{Sm}(\text{tta-Si})_3(\text{phen})_2$ and $\text{Sm}(\text{phen-Si})_3(\text{tta})_2$ complexes. The luminescence of the Sm^{3+} ion occurs in three regions of the visible electromagnetic spectrum, 560 nm (${}^4\text{G}_{5/2}\rightarrow{}^6\text{H}_{5/2}$), 595 nm (${}^4\text{G}_{5/2}\rightarrow{}^6\text{H}_{7/2}$), and 645 nm (${}^4\text{G}_{5/2}\rightarrow{}^6\text{H}_{9/2}$). The emission peaks correspond to the transitions from the ${}^4\text{G}_{5/2}$ level to different J levels, with the ${}^6\text{H}$ (${}^6\text{H}; J = 5/2 - 15/2$) and ${}^4\text{F}$ (${}^4\text{F}; J = 5/2 - 11/2$). The most intense transition is ${}^4\text{G}_{5/2}\rightarrow{}^6\text{H}_{9/2}$ (645 nm) of magnetic dipole character. [13] Here, for both $\text{Sm}(\text{tta-Si})_3(\text{phen})_2$ and $\text{Sm}(\text{phen-Si})_3(\text{tta})_2$ complexes these transitions appears slightly shifted in 565 nm (${}^4\text{G}_{5/2}\rightarrow{}^6\text{H}_{5/2}$), 605 nm (${}^4\text{G}_{5/2}\rightarrow{}^6\text{H}_{7/2}$), 648 nm (${}^4\text{G}_{5/2}\rightarrow{}^6\text{H}_{9/2}$), and 708 nm (${}^4\text{G}_{5/2}\rightarrow{}^6\text{H}_{11/2}$). The most common transitions in the excitation spectrum of the Sm^{3+} ions are weak, generally overshadowed by the organic ligand bands. [13] Nevertheless, here, the ${}^6\text{H}_{5/2}\rightarrow{}^6\text{P}_{5/2}$ (418 nm) and ${}^6\text{H}_{5/2}\rightarrow{}^6\text{G}_{7/2}$ (461 nm) transitions remain visible and slightly shifted in the excitation spectra.

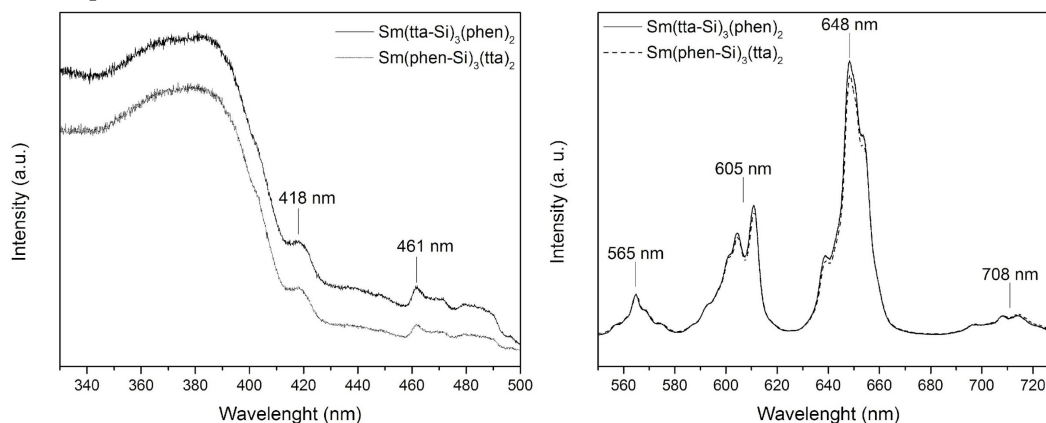


Figure 1. Luminescence spectra (excitation - left, and emission - right) of the $\text{Sm}(\text{tta-Si})_3(\text{phen})_2$ and $\text{Sm}(\text{phen-Si})_3(\text{tta})_2$ complexes, acquired with slit widths exc/em = 2/2 mm; increment = 0.5 nm; speed = 0.1 s.

For the three obtained silylated complexes of Eu^{3+} , the excitation and emission spectra are presented in Figure 2. In this study, the excitation spectrum was centered at a wavelength of 613 nm , corresponding to the ${}^5\text{D}_0\rightarrow{}^7\text{F}_2$ transition of the Eu^{3+} ion. This transition, dominant and more intense compared to others in the emission spectrum, suggests a site with reduced symmetry without an inversion center. [14] Other transitions typically observed for this ion in the emission spectrum are also attributed to ${}^5\text{D}_0\rightarrow{}^7\text{F}_J$ ($J=0-4$): ${}^5\text{D}_0\rightarrow{}^7\text{F}_0$ (580 nm); ${}^5\text{D}_0\rightarrow{}^7\text{F}_1$ (594 nm); ${}^5\text{D}_0\rightarrow{}^7\text{F}_3$ (650 nm); and ${}^5\text{D}_0\rightarrow{}^7\text{F}_4$ (701 nm). [14] These transitions correspond to the intra-energetic level $4f^6$ of the Eu^{3+} ion. [15] The dipole-magnetic transition ${}^5\text{D}_0\rightarrow{}^7\text{F}_1$ is known to be allowed and insensitive to the chemical environment, whereas ${}^5\text{D}_0\rightarrow{}^7\text{F}_2$ is forbidden and hypersensitive to the environment. When the Eu^{3+} ion is doped, for instance, this transition indicates high symmetry with an inversion center, whereas when it is inserted into inorganic matrices, it exhibits reduced symmetry sites. [14] If the ${}^5\text{D}_0\rightarrow{}^7\text{F}_2$ transition is much more intense than ${}^5\text{D}_0\rightarrow{}^7\text{F}_1$, then the complex will emit pure red light. [16]

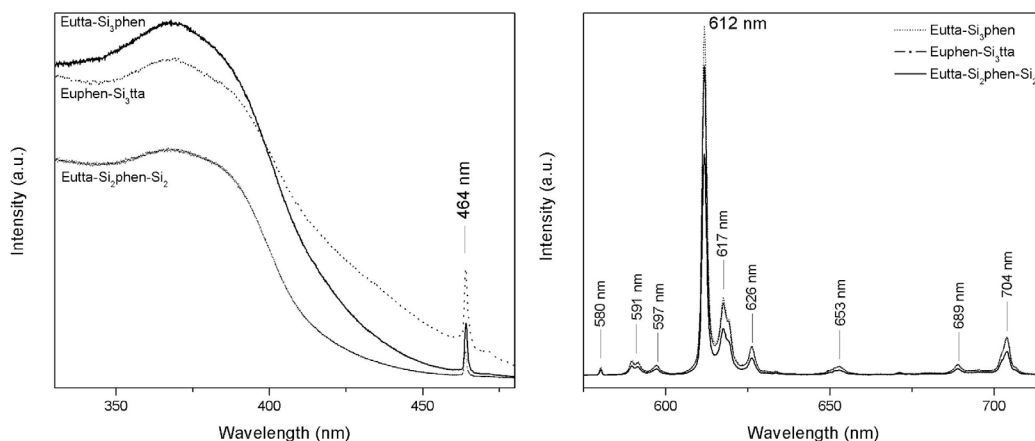


Figure 2. Luminescence spectra (excitation - left, and emission - right) of the $\text{Eu}(\text{tta-Si})_3(\text{phen})$, $\text{Eu}(\text{phen-Si})_3(\text{tta})$, and $\text{Eu}(\text{tta-Si})_2(\text{phen-Si})_2$ complexes, acquired with slit widths exc/em = 2/2 mm; increment = 1 nm; speed = 0.1 s.

The luminescence decay is a parameter crucially important because it provides information about the efficiency and dynamics of the luminescent process in lanthanide complexes. Long luminescence lifetimes are often observed in lanthanide complexes due to the forbidden nature of $f-f$ transitions, which leads to slow radiative decay rates. Herein, the observed luminescence lifetime for the Sm^{3+} and Eu^{3+} silylated complexes synthesized (Table 1) varied between 0.070 ms (Sm^{3+} complexes) to > 0.50 ms (Eu^{3+} complexes) values.

Table 1. Experimental Lifetimes (τ_{exp}) acquired for the Sm^{3+} and Eu^{3+} silylated complexes obtained.

Silylated complex	$\tau_{\text{exp}}(\text{ms})$	Observed Transition
$\text{Sm}(\text{tta-Si})_3(\text{phen})_2$	0.070	${}^4\text{G}_{5/2} \rightarrow {}^6\text{H}_{9/2}$ ¹
$\text{Sm}(\text{phen-Si})_3(\text{tta})_2$	0.071	
$\text{Eu}(\text{tta-Si})_3(\text{phen})$	0.80	${}^5\text{D}_0 \rightarrow {}^7\text{F}_2$ ²
$\text{Eu}(\text{phen-Si})_3(\text{tta})$	0.72	
$\text{Eu}(\text{tta-Si})_2(\text{phen-Si})_2$	0.59	

¹ $F_{\text{exc}3}/F_{\text{em} 2}$; 150 flash count; initial time 0.005 nm; inc 0.01 nm. ² $F_{\text{exc/em} 1}$; 150 flash count; initial time 0.005 nm; inc 0.01 nm.

The shape of the emission spectrum, i.e., the ratios of integrated emission intensities $I({}^5\text{D}_0 \rightarrow {}^7\text{F}_J, J = 0 \text{ to } 4)$ to $I({}^5\text{D}_0 \rightarrow {}^7\text{F}_1)$ may be used to calculate the radiative rate, the $A_{\text{rad}} = \sum A_{0 \rightarrow j}$ and the Ω_2 and Ω_4 Judd-Ofelt intensity parameters, which give indications about the average local field at the europium ion. Details of the calculation have been given by Ćirić et al. (2019). [17] The experimental intensity parameters were also calculated, and the results (Table 2) obtained for the complexes were very similar, the high values found for Ω_2 traduces the high intensity of the hypersensitive transition ${}^5\text{D}_0 \rightarrow {}^7\text{F}_2$ and means that the site occupied by the Eu^{3+} ion is not centrosymmetric, and that the ligand field is strongly polarizing. The other value of interest is the ${}^5\text{D}_0$ radiative lifetime τ_{rad} . By comparing the observed lifetime (τ_{exp}) with the radiative one, the ${}^5\text{D}_0$ emission quantum efficiency ($q = \tau_{\text{exp}}/\tau_{\text{rad}}$) is calculated. The luminescence decay curves, with emission monitored at ${}^5\text{D}_0 \rightarrow {}^7\text{F}_2$, could be fitted by a monoexponentially decay function. These found values for q suggests that the coordination sphere of the europium is here stabilized by intramolecular interactions of the nearby ethoxy functions of the pending group of the tta and phen ligands. [5]

Table 2. Judd-Ofelt Intensity Parameters (Ω_2 , Ω_4), Radiative Rates (A_{rad}), Radiative and Experimental Lifetimes (τ_{rad} , τ_{exp}), and Quantum Efficiencies (q).

Silylated complex*	Ω_2 ($\times 10^{-20}$ cm ²)	Ω_4 ($\times 10^{-20}$ cm ²)	A_{rad} (s ⁻¹)	τ_{exp} (ms)	q
Eu(tta-Si)₃(phen)	18.20	6.63	248.7	3.21	0.80
Eu(phen-Si)₃(tta)	18.34	6.56	250.7	3.19	0.72
Eu(tta-Si)₂(phen-Si)₂	17.97	6.78	245.7	3.23	0.59

*Values obtained using JOES software developed by Ćirić et al. (2019) [17].

2.2. Silica Nanoparticles Containing Silylated Sm³⁺ and Eu³⁺ Complexes

After characterizing the synthesized silylated complexes of Sm³⁺ and Eu³⁺, only Sm(tta-Si)₃(phen)₂ and Eu(tta-Si)₃(phen) were the selected complexes for the next step of incorporation into the silica nanoparticles.

Observing Table 3, it is noticeable that the mesoporous silica nanoparticles containing the complexes Sm(tta-Si)₃(phen)₂ and Eu(tta-Si)₃(phen) have very similar D_h values. The insertion of the complexes does not significantly alter their size, which ranges between 250 and 280 nm. In contrast, the dense silica nanoparticles containing the complexes Sm(tta-Si)₃(phen)₂ and Eu(tta-Si)₃(phen) have very similar D_h values, varying from 40 to 90 nm. Regarding the obtained ZP values, it is noted that this set of nanoparticles is not stable in deionized water at pH 6.5, as all the ZP values fall between +30 mV and -30 mV. Therefore, they tend to aggregate in the medium, which explains the high D_h values.

Table 3. DLS values for the hydrodynamic diameter and Zeta Potential (ZP) of mesoporous silica nanoparticles (MSNs and DSNs) and silica nanoparticles containing the complexes Sm(tta-Si)₃(phen)₂ and Eu(tta-Si)₃(phen).

Sample	D_h (nm)	ZP (mV)*
MSNs	230 ±86	-24,3 ±8,7
SiO₂m@Sm(tta-Si)₃(phen)₂	280 ±48	-15,3 ±5,3
SiO₂m@Eu(tta-Si)₃(phen)	255 ±47	-14,3 ±5,4
DSNs	79 ±64	-11,5 ±7,0
SiO₂d@Sm(tta-Si)₃(phen)₂	43 ±6	-26,1 ±6,83
SiO₂d@Eu(tta-Si)₃(phen)	76 ±21	-15,7 ±4,57

* D_h denotes Hydrodynamic Diameter. ZP values obtained in pH 6.5.

The SAXS curves presented in Figure S2 are characteristic of hexagonal MCM-41 material with a well-organized mesostructure [18], showing visible diffraction peaks $d_{(100)}$, $d_{(110)}$, $d_{(200)}$, and $d_{(210)}$ for the mesoporous SiO₂ curve. These diffraction peaks correspond to the correlation distances from the center of one pore to another in porous materials. With the information on the pore correlation distances, it is possible to outline a profile of how the porous network is organized on the material's surface. For MCM-41 type mesoporous silica, the pore organization profile on its surface is hexagonal. It is noted that when the complexes are incorporated into the silica particles, there is a shift in the diffraction peaks compared to the diffraction peaks of the mesoporous SiO₂ sample without complexes. The intensity of these peaks decreases, and the $d_{(200)}$ and $d_{(210)}$ peaks disappear in the SiO₂m@Sm(tta-Si)₃(phen)₂ curve, and $d_{(210)}$ disappears in the SiO₂m@Eu(tta-Si)₃(phen) curve, confirming the successful incorporation of the complexes into the silica nanoparticles. The electron density on the particle surface changes with the incorporation of the complexes, and the diffraction pattern is thus altered.

According to Table 4, the specific surface area calculated was 913.3 m² g⁻¹ for the MSNs with average pore size found of 4.78 nm, and total pore volume estimated of 1.09 cm³ g⁻¹, while the nanoparticles containing the silylated complexes showed lower values for these parameters, which

confirms the other results (SAXS, DLS and ZP) that the incorporation of these complexes into the silica nanoparticles was successful.

Table 4. Values for porosity and surface area measurements of the MSNs, SiO₂m@Sm(tta-Si)₃(phen)₂, SiO₂m@Eu(tta-Si)₃(phen), SiO₂d@Sm(tta-Si)₃(phen)₂, and SiO₂d@Eu(tta-Si)₃(phen).

Sample	$a_{s,BET}$ (m ² g ⁻¹)*	D _{pores} (nm)	V _{pores} (p/po) ₁ (cm ³ g ⁻¹)	a _{pore,BJH} (m ² g ⁻¹)**
MSNs	913.29	4.78	1.09	962.75
SiO ₂ m@Sm(tta-Si) ₃ (phen) ₂	408.43	4.15	0.42	269.74
SiO ₂ m@Eu(tta-Si) ₃ (phen)	442.36	4.16	0.46	403.33
SiO ₂ d@Sm(tta-Si) ₃ (phen) ₂	157.07	11.29	0.44	159.46
SiO ₂ d@Eu(tta-Si) ₃ (phen)	229.69	7.86	0.45	242.78

* Values of surface area measurements acquired using Brunauer-Emmett-Teller (BET) method. ** Values of porosity measurements acquired using Barrett-Joyner-Halenda (BJH) method.

In the TEM images shown in Figure 3, the MSNs (a) and DSNs (b) are presented. For the MSNs, the image reveals the well-ordered pore structure of the nanoparticles, evidenced by the contrast differences, confirming the SAXS analysis results. The scale also indicates that the nanoparticles have a size arrangement close to 100 nm, which is smaller than the D_h estimated by the DLS analysis. For the DSNs, the image exhibits particle size smaller than 50 nm and high level aggregation, confirming the obtained results in DLS measurements.

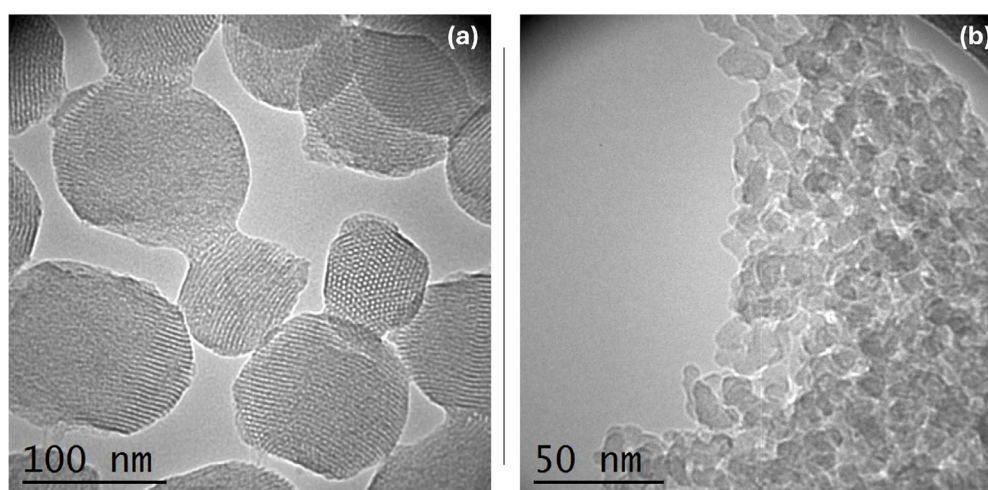


Figure 3. Images of the (a) MSNs from Transmission Electron Microscopy, obtained at 66 kV, and (b) DSNs from Transmission Electron Microscopy, obtained at 115 kV.

Figures 4 and 5 show images of SiO₂m@Sm(tta-Si)₃(phen)₂ and SiO₂m@Eu(tta-Si)₃(phen) with their respective EDX analyses and particle size distribution histograms. It is observed that the morphology of the nanoparticles varies from spherical to oval. The nanoparticles appear aggregated, which was already evidenced by the previously presented DLS and ZP measurements. Here, the estimated size of the NPs is smaller (130 - 150 nm) than the size found in the DLS measurements (230 - 280 nm). The EDX microanalysis reveals the presence of Ln³⁺ ions in smaller proportions than Si and O, as expected, confirming the successful incorporation of the complexes into the MSNs.

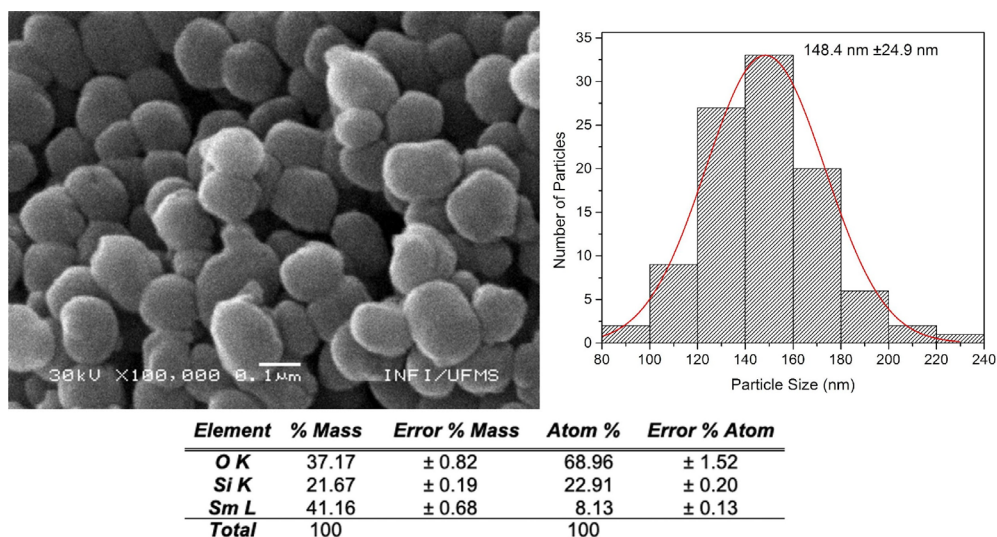


Figure 4. SEM image with a Histogram of the size distribution versus the number of nanoparticles counted, and EDX analysis of $\text{SiO}_2\text{m@Sm}(\text{tta-Si})_3(\text{phen})_2$.

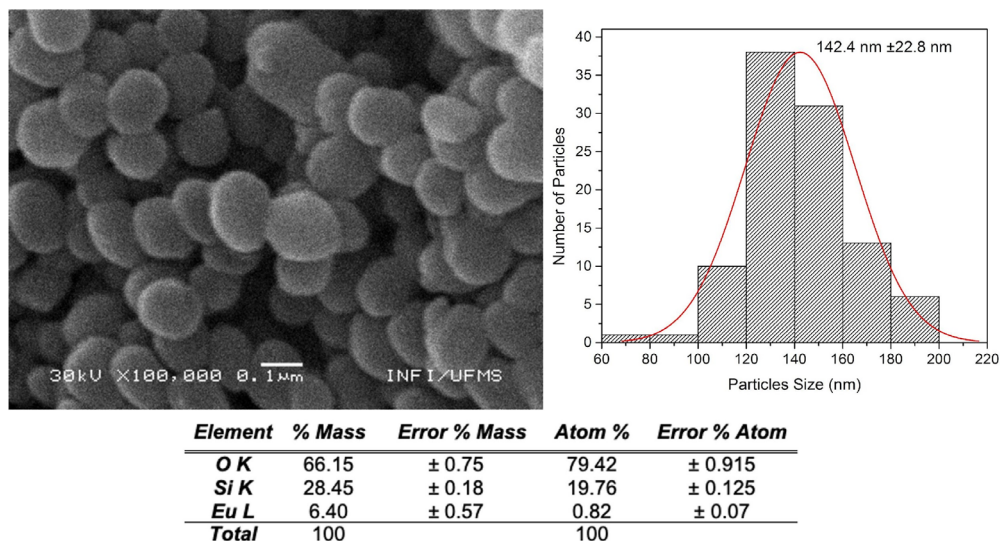


Figure 5. SEM image with a Histogram of the size distribution versus the number of nanoparticles counted, and EDX analysis of $\text{SiO}_2\text{m@Eu}(\text{tta-Si})_3(\text{phen})_2$.

The SEM images presented in Figures 6, and 7 correspond respectively to $\text{SiO}_2\text{d@Sm}(\text{tta-Si})_3(\text{phen})_2$, and $\text{SiO}_2\text{d@Eu}(\text{tta-Si})_3(\text{phen})_2$, with their respective size distribution histograms. The morphology of the nanoparticles before (seen by TEM image in Figure 3b) and after the insertion of the complexes remains practically unchanged, exhibiting a spherical pattern. All samples appear aggregated, which is corroborated by the DLS and ZP results. Despite this, the observed particle size (55 - 70 nm) is very similar to that determined by DLS measurements (40 - 80 nm), as the size determined by DLS is apparent due to the D_h and can vary larger or smaller compared to the actual size.

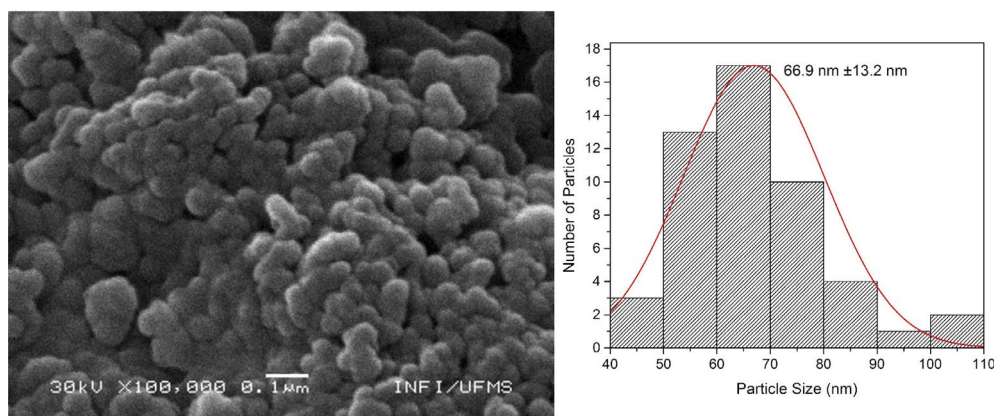


Figure 6. SEM image with a Histogram of the size distribution versus the number of nanoparticles counted of $\text{SiO}_2\text{d}@Sm(\text{tta-Si})_3(\text{phen})_2$.

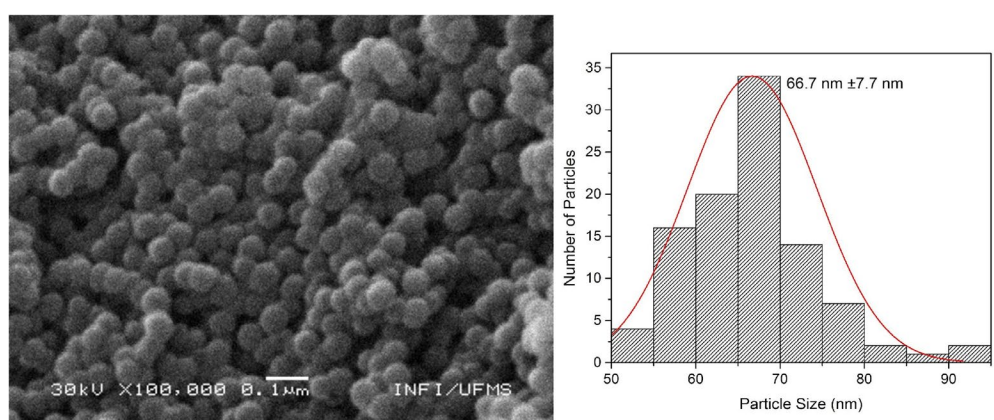


Figure 7. SEM image with a Histogram of the size distribution versus the number of nanoparticles counted of $\text{SiO}_2\text{d}@Eu(\text{tta-Si})_3(\text{phen})$.

The luminescence measurements performed on the nanoparticles incorporated with Sm^{3+} and Eu^{3+} silylated complexes, when incorporated in the MSNs do not show very significant differences compared to the same free complexes characterized (Figures S3-S4). An exception, however, observed for $\text{SiO}_2\text{d}@Eu(\text{tta-Si})_3(\text{phen})$ appears to have undergone significant deterioration during its incorporation into the dense silica nanoparticles (Figure S5), while $\text{SiO}_2\text{d}@Sm(\text{tta-Si})_3(\text{phen})_2$ did not showed any luminescence at all.

Cell death occurred with the increase in concentration of Sm^{3+} and Eu^{3+} complexes (Figure S6) in all tested cell lines, with a greater reduction in cell viability starting at a concentration of $10.96 \mu\text{g mL}^{-1}$. Among the tumor cells, the most sensitive to the Sm^{3+} and Eu^{3+} complexes were the A431 line (Table 5). The NIH3T3 cell line was the least sensitive to the tested complexes. $\text{SiO}_2\text{m}@Eu(\text{tta-Si})_3(\text{phen})$ caused cell death starting at a concentration of $10.98 \mu\text{g mL}^{-1}$ (Figure S7a), with tumor lines being more sensitive, causing the death of more than 50% of the cells. $\text{SiO}_2\text{m}@Eu(\text{tta-Si})_3(\text{phen})$ showed low toxicity to the NIH3T3 line compared to the tested tumor lines, with about 40% cell death, which is evidenced by the higher IC_{50} value (Table 5). $\text{SiO}_2\text{m}@Sm(\text{tta-Si})_3(\text{phen})_2$ (Figure S7b) caused a maximum of 25% cell death at most tested concentrations. At concentrations above $90 \mu\text{g mL}^{-1}$, cell death reached 50%, with the B16F10 line being the most sensitive (Table 5).

Table 5. IC₅₀ values of Sm(tta-Si)₃(phen)₂, Eu(tta-Si)₃(phen), SiO₂m@Sm(tta-Si)₃(phen)₂, and SiO₂m@Eu(tta-Si)₃(phen) on NIH-3T3 (healthy murine fibroblast cells), 4T1 (mammary carcinoma BALB/cfC3H mice), B16F10 (murine melanoma), and A431 (human epidermoid carcinoma) cell lines after 24 hours of treatment.

Sample*	Cell lines (IC ₅₀ µg mL ⁻¹)			
	4T1	B16F10	A431	NIH-3T3
Eu(tta-Si) ₃ (phen)	30.8	45.3	15.3	87.0
SiO ₂ m@Sm(tta-Si) ₃ (phen) ₂	40.9	49.9	24.7	108.8
Sm(tta-Si) ₃ (phen) ₂	34.6	24.9	9.8	-
SiO ₂ m@Eu(tta-Si) ₃ (phen)	195.3	169.6	102.7	236.5

*All samples were dissolved in DMSO before preparing the solutions at the concentrations specified in the table, in supplemented culture medium.

3. Discussion

Fluorescence and emission intensity of Ln³⁺ complexes significantly increase upon the insertion of a second organic ligand, which acts as an energy donor, thereby enhancing fluorescence intensity in Ln³⁺ binary complexes (synergistic effect). This enhancement assists in completing the coordination sphere of Ln³⁺ ions. [15] As a result, most of the designed complexes feature two ligands. The Sm³⁺ ion emits in three regions of the visible electromagnetic spectrum: green at 560 nm (⁴G_{5/2}→⁶H_{5/2}), orange at 595 nm (⁴G_{5/2}→⁶H_{7/2}), and red at 645 nm (⁴G_{5/2}→⁶H_{9/2}). These emission peaks correspond to *f-f* transitions from the ⁴G_{5/2} level to different J levels with 6H terms (⁶H_J, J= 5/2 to 15/2) and 4G (⁴G_J, J= 5/2 to 11/2). The most intense transition is the ⁴G_{5/2}→⁶H_{9/2} (645 nm), which has a dipole electric character and is hypersensitive [13], while the others are ⁴G_{5/2}→⁶H_{5/2} (magnetic dipole), ⁴G_{5/2}→⁶H_{7/2} (magnetic dipole), and ⁴G_{5/2}→⁶H_{11/2} (705 nm, magnetic dipole), which typically broaden. [13,19–21] The most common excitation transitions for the Sm³⁺ ion is ⁶H_{5/2}→⁴D_{3/2} (360 nm), ⁶H_{5/2}→⁴D_{1/2} (375 nm), and ⁶H_{5/2}→⁶P_{5/2} (405 nm), which appear as narrow peaks with weak intensity. These transitions are often masked by the absorption bands of the organic ligands, with only the ⁶H_{5/2}→⁴M_{19/2} (465 nm) transition being observed in the complexes presented here. [13]

Eu³⁺ complexes, in general, exhibit high quantum efficiency and a versatile coordination environment. [16] Due to these properties, we used this ion in this work. The most intense and dominant transition in the emission spectrum for the Eu³⁺ ion is ⁵D₀→⁷F₂ (613 nm). This transition indicates a site of reduced symmetry without an inversion center. [14] Other transition peaks correspond to the is ⁵D₀→⁷F_J (J = 0 to 4): is ⁵D₀→⁷F₀ (580 nm), is ⁵D₀→⁷F₁ (594 nm), is ⁵D₀→⁷F₃ (650 nm), and is ⁵D₀→⁷F₄ (701 nm) (CHOI et al., 2015), which are related to the intra-energetic level 4f⁶ of the Eu³⁺ ion. (LI et al., 2013) The transition with dipole magnetic character, is ⁵D₀→⁷F₁, is known to be allowed and hypersensitive to the environment. If the ⁵D₀→⁷F₂ transition is more intense than the ⁵D₀→⁷F₁ transition, then the complex will emit pure red light [16], as observed in our silylated complexes. In the excitation spectra, a broad band can be observed, which is related to the energy transfer from the oxygen/nitrogen 2p orbitals in the ligands to the 4f empty orbital of the Eu³⁺ ion. [16]

In DLS, D_h can be defined as the size of a rigid particle that diffuses through the medium in the same way as the particle being measured, assuming a hydration layer around it. This is because, in solution, a particle is not completely spherical; it is dynamic and solvated. Therefore, the diameter measured by the equipment will be an indicative apparent size calculated from the diffusion properties of the particles. The measured volume percentage relates to the distribution of the relative proportion of various components in a sample based on their mass and volume. This means it represents the quantity of particles in the peaks of highest intensity of measured D_h. [22]

The Zeta Potential (ZP) is a key indicator of particle stability in colloidal suspensions, as it shows the degree of electrostatic dispersion between adjacent, similarly charged particles. In very small particles, a high ZP value indicates good stability, meaning they will not aggregate easily in the

medium. When the ZP value is low, the attractive forces in the medium may overcome the particle repulsion, breaking the dispersion and causing the particles to aggregate, indicating low stability in the medium. Generally, particles with ZP values between +30 mV and -30 mV are considered unstable, while particles with values greater than ± 30 mV are considered stable. [22]

The most important factor directly influencing ZP values is pH, as the addition of acid or base to the suspension and/or dispersion changes the particle charge in the medium, consequently altering the ZP value of the particles. Another consideration is that we can easily confirm the different stages in the development of these NPs through the different ZP values obtained. As new compounds are added to the silica NPs, the ZP value shifts from smaller negative values to higher positive values in mV, then drops to smaller but positive values. This behavior is different from that observed in mesoporous silica NPs, as they are different types of silica and the Ln^{3+} complexes are incorporated differently in each type of silica.

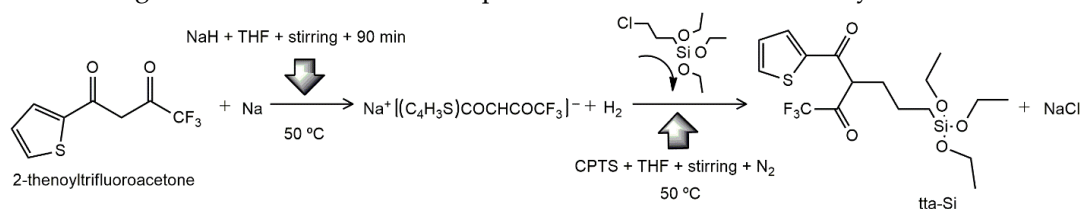
4. Materials and Methods

Tetrahydrofuran anhydrous (THF), 3-chloropropyl-triethoxysilane (CPTS), sodium hydrate (NaH), 2-thenoyltrifluoroacetone (TTA), 1,10-phenanthroline monohydrate (1,10-phen), and phosphate buffer saline (PBS) were purchased from Sigma Aldrich. Dimethyl sulfoxide (DMSO, 99.9%) from J.T Baker; ethanol anhydrous from Dinâmica; Dulbecco's Modified Eagle Medium (DMEM) containing 10% fetal bovine serum (FBS) from Gibco; Trypsin/EDTA from Gibco; Bovine serum albumin (BSA) from Life Technologies; penicillin, streptomycin 100 $\mu\text{g}/\text{mL}$ - STR/PEN from Life Technologies; (3-(4,5-dimethylthiazol-2-yl)-2,5-diphenyltetrazolium bromide (MTT) from Life Technologies; and Nitrogen gas from White Martins. All reagents were of analytical grade and were used as received without further purification and throughout the experiments Milli-Q grade water (Millipore system) was used. Samarium nitrate, $\text{Sm}(\text{NO}_3)_3$, and Europium nitrate, $\text{Eu}(\text{NO}_3)_3$, solutions were obtained by salts of Samarium and Europium Oxide, whose purity is higher than 99%.

4.1. Ligand Silylation with 3-chloropropyl-triethoxysilane (CPTS)

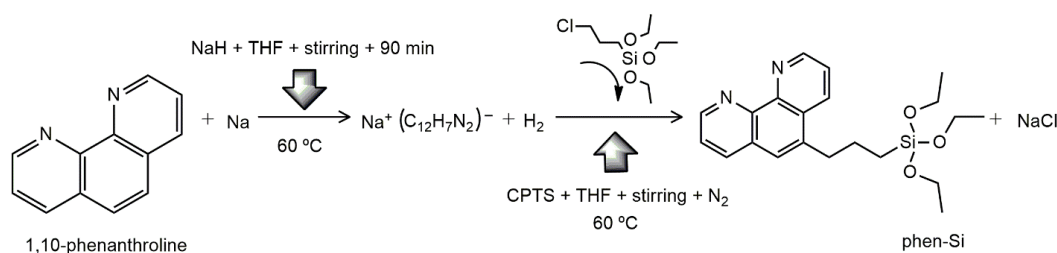
To obtain silylated complexes of Sm^{3+} and Eu^{3+} , the organic ligand 2-thenoyltrifluoroacetone (tta) and 1,10-phenanthroline monohydrate (phen) were modified by a silylation reaction. Based on experimental procedures of Qiao and Yan (2009) [23], and Duarte et al. (2012) [5], these syntheses were performed with modifications on reactants amount, temperature of synthesis and using 3-chloropropyltriethoxysilane (3-CPTS) as silylating agent.

Then, in a dry flash, 2 mmol of tta were added to 20 mL of anhydrous tetrahydrofuran under stirring at 50 °C. After, 2 mmol of sodium hydrate (NaH) were slowly added to the mixture under the N_2 atmosphere. The mixture was stirred over 90 min, under N_2 atmosphere at 50 °C. Finally, 2 mmol of 3-CPTS were added dropwise to reaction. This step was kept by 18 h, under stirring, N_2 atmosphere at 50 °C. The obtained product was washed with diethyl ether, filtered and dry under vacuum overnight at 30 °C. The **Scheme 1** represents tta modification. Mass yield was 63.88%.



Scheme 1. Synthesis of tta-Si from reaction between 2-thenoyltrifluoroacetone (tta) and 3-chloropropyltriethoxysilane (3-CPTS) as silylating agent.

Same procedure was used for 1,10-phenanthroline modification, except temperature which was increased to 60 °C (seen in the Scheme 2). Mass yield was 40.55 %.



Scheme 2. Synthesis of phen-Si from reaction between 1,10-phenanthroline monohydrate (phen) and 3-chloropropyltriethoxysilane (3-CPTS) as silylating agent.

4.2. Synthesis of Silylated Sm^{3+} and Eu^{3+} Complexes

Silylated Sm^{3+} complexes were aimed with a 10-coordination number (ligand:metal ratio), since this coordination sphere is the most probable for Sm^{3+} . Whereas silylated Eu^{3+} complexes were aimed with an 8-coordination number, most probable coordination sphere for Eu^{3+} .

Basically, silylated complexes were performed by mixing of silylated ligand, non silylated ligand, $\text{Ln}(\text{NO}_3)_3$ solution (where $\text{Ln} = \text{Sm}$ or Eu), and anhydrous ethanol. All reactions were maintained by 18 h, under stirring, N_2 atmosphere and 50°C . At the end of each complex synthesis, the solvent was evaporated, the precipitate was washed with pentane and diethyl ether, and dried under vacuum overnight at 30°C .

Average mass yield varied widely, and the values were: 42.05% for $\text{Sm}(\text{tta-Si})_3(\text{phen})_2$; 28.31% for $\text{Sm}(\text{phen-Si})_3(\text{tta})_2$; 63.14% for $\text{Eu}(\text{tta-Si})_3(\text{phen})$; 56.1% for $\text{Eu}(\text{phen-Si})_3(\text{tta})$; and 41.06% for $\text{Eu}(\text{tta-Si})_2(\text{phen-Si})_2$.

4.3. Synthesis of Mesoporous Silica Nanoparticles (MSNs)

The synthesis procedure used was inspired by the work of He et al. (2010) [24], in which sodium hydroxide (NaOH) and cetyltrimethylammonium bromide (CTAB) were mixed in distilled water. The mixture was then kept under constant stirring at 80°C . Subsequently, tetraethyl orthosilicate (TEOS), a silica precursor, was added dropwise. The mixture was kept under vigorous stirring for 20 hours at 80°C . Finally, the resulting precipitated material was centrifuged and washed several times with distilled water. The centrifuged product was dried in an oven at $50 - 70^\circ\text{C}$ and then calcined to completely remove the surfactant. [3]

4.4. Insertion of Ln^{3+} Silylated Complexes into MSNs ($\text{SiO}_2\text{m@silylated Complex}$)

We used a modified protocol based on the one we previously proposed [25]. Calcined mesoporous silica nanoparticles and $\text{Sm}(\text{tta-Si})_3(\text{phen})_2$ were mixed in ethanol. This mixture was kept under agitation for 24 h at room temperature. Finally, the product was centrifuged and dried under vacuum at room temperature to avoid degradation of the complex. The supernatant was not discarded to perform chemical analysis by titration. The same procedure was used for the insertion of the $\text{Eu}(\text{tta-Si})_3(\text{phen})$ complex into the MSNs.

4.5. Synthesis of Dense Silica Nanoparticles (DSNs)

The synthesis of these nanoparticles utilized a reverse microemulsion reaction of water in oil. According to Zhao et al. (2004) [26] and Cousinié et al. (2012) [1], the operational protocol involved reacting cyclohexane (oil phase), n-octanol (reaction co-solvent), and Triton X-100 under vigorous stirring for 15 min to create and stabilize the microemulsion. Deionized water was then added dropwise to avoid breaking the microemulsion. Very vigorous stirring (1050 rpm) for 20 min was required to stabilize the microemulsion. Then, TEOS was added dropwise, followed by 10 minutes of vigorous stirring. Finally, ammonium hydroxide (NH_4OH , 25%) was added dropwise. The reaction was maintained under vigorous stirring at 1050 rpm for 24 h at 22°C .

At the end of the process, acetone was added to the reaction flask, and the mixture was stirred for 15 min at 1050 rpm to allow the acetone to "break" the microemulsion. The mixture was then left to rest for 2 h to ensure the decantation of the DSNs. The precipitated product was dialyzed in deionized water for 3 days in a thermostatic bath under stirring with periodic water changes. After dialysis, the DSNs were centrifuged and washed several times with ethanol, deionized water, acetonitrile, and diethyl ether, and finally dried in a vacuum oven for 12 h at 40 °C.

4.6. Insertion of Ln^{3+} Silylated Complexes into DSNs ($\text{SiO}_2\text{d@silylated Complex}$)

The insertion of $\text{Sm}(\text{tta-Si})_3(\text{phen})_2$ and $\text{Eu}(\text{tta-Si})_3(\text{phen})$ complexes into DSNs was carried out during the synthesis of the NPs by co-precipitation. The complexes were pre-solubilized in the portion of deionized water used in the reaction and added to the mixture during the water addition step. The other steps of the procedure are described in Section 2.4.

4.7. Characterization

Fourier Transform Infrared Spectroscopy (FTIR): The FTIR spectra were obtained by a Nicolet iS5 model from Thermo Fisher Scientific, ranging from 4000-400 cm^{-1} , 4 cm^{-1} of resolution, 100 scans min^{-1} , and diluted in KBr pellets with 1% (w/w) final concentration.

Luminescence Spectroscopy and Luminescence Decay: were performed using a spectrofluorimetric Horiba Jobin-Yvon FluoroLog-3 with Xe lamp of 450 W, as excitation source, monochromator iHR-320, under the same instrumental conditions for all samples. The samples are used in a solid state, the signals were normalized by excitation lamp power, and the emissions were corrected (slit and increment values are shown in each spectrum graphic). For luminescence decay, a pulsed Xe lamp was used, the most intense transition was used as λ_{em} , for Sm^{3+} complexes the transition was ${}^4\text{G}_{5/2} \rightarrow {}^6\text{H}_{9/2}$ (650 nm) and for Eu^{3+} complexes the transition was ${}^5\text{D}_0 \rightarrow {}^7\text{F}_2$ (612 nm). Data acquisition parameters were the same for all samples: integration time between pulses of 0.01 ms, initial delay of 0.005 ms, maximum delay of 2 ms, cycling time of 51 ms, number of pulses of 150 per cycle.

Dynamic Light Scattering (DLS) and Zeta Potential (ZP): DLS and ZP measurements were performed to determine the hydrodynamic diameter (DH) and surface charge of the nanoparticles, respectively. These measurements were carried out using a Malvern Instruments Zetasizer Nano ZS Series device, with deionized water as the dispersing solvent and using appropriate cuvettes for each type of measurement.

Small-Angle X-ray Scattering (SAXS): The SAXS spectra of the MSNs and $\text{SiO}_2\text{m@silylated}$ complex nanoparticles were obtained using an INEL XRG3D instrument. The SAXS signal of the nanoparticles (NPs) was obtained with X-rays produced by a Cu anode. Measurements were carried out with a 1x1 mm beam, and an image plate detector located 38 cm from the sample, with an acquisition time of 1 h. In the measurement device, the beam formatting is provided by Kirkpatrick-Baez mirrors, followed by two crossed slits (horizontal and vertical). This technique provides information on the pore arrangement in the NPs, through X-ray scattering due to differences in the electronic densities of the atoms composing the NPs, making it possible to confirm the modification and insertion of complexes into the mesoporous silica NPs by analyzing changes in the spectra.

Porosity and Surface Area Measurements: Surface area measurements by the Brunauer-Emmett-Teller (BET) method and porosity measurements by the Barrett-Joyner-Halenda (BJH) method were obtained using N_2 adsorption-desorption to determine the pore size and shape, as well as the surface area of the NPs. These measurements were conducted using a Micromeritics ASAP2020 porosimeter.

Scanning and Transmission Electron Microscopy (SEM and TEM) and Energy-Dispersive X-ray Spectroscopy (EDX): Transmission Electron Microscopy (TEM) images were taken using a Phillips CM20 high-voltage microscope operating at up to 200 kV, with a LaB6 electron source. The samples were dispersed in ethanol and sonicated before deposition and drying on Cu grids coated with a carbon film (300 mesh), specific for TEM imaging. In addition to TEM images, scanning electron microscopy with energy-dispersive X-ray spectroscopy (SEM/EDX) images were also obtained using a JEOL JSM-6380LV microscope with an attached Thermo Scientific Noran System Six EDX

spectrometer. Powder samples were deposited on carbon tape without any prior preparation, and after EDX measurements, they were sputter-coated with Au to achieve better contrast in the images.

MTT Assay for Cytotoxicity and Cell Viability: The cells used in this assay were NIH-3T3 adherent cell lines (healthy murine fibroblast cells), 4T1 (mammary carcinoma BALB/cfC3H mice), B16F10 (murine melanoma), and A431 (human epidermoid carcinoma), kindly supplied by the Laboratory of Nanobiotechnology at the Genetic and Morphology Department of the Institute of Biology, University of Brasília, Brasília-DF, Brazil. The assay methodology carried out was based on Mosmann (1983) [27]. The cells were cultured in Dulbecco's Modified Eagle's Medium (DMEM) supplemented with 10% fetal bovine serum (FBS) and 1% antibiotics (Penicillin/Streptomycin), all from Gibco® by Life Technologies, maintained in an incubator at 37 °C with 5% CO₂. For the experiments, the cells were detached from the culture flasks using trypsin-EDTA (0.05%), also from Gibco® by Life Technologies, for 3 min in the incubator, collected in 15 mL conical tubes, centrifuged at 2000 rpm for 3 min, resuspended in DMEM, counted using a Neubauer chamber, and plated in 96-well plates at a cell concentration of 3.10³ cells per well. After 24 h of plating, the cells were incubated with culture medium containing different concentrations (25 µg mL⁻¹; 20 µg mL⁻¹; 15 µg mL⁻¹; 10 µg mL⁻¹; and 5 µg mL⁻¹) of the complexes: Sm(tta-Si)₃(phen)₂ and Eu(tta-Si)₃(phen); and the NPs of: SiO₂m@Sm(tta-Si)₃(phen)₂, SiO₂m@Eu(tta-Si)₃(phen), SiO₂d@Sm(tta-Si)₃(phen)₂, SiO₂d@Eu(tta-Si)₃(phen), dispersed in a maximum of 1% dimethyl sulfoxide (DMSO), in triplicate, for a period of 24 h. Supplemented DMEM medium was used as a negative control. After the incubation period, the medium was discarded, and each well was washed by adding a phosphate-buffered saline (PBS) solution. After washing, 150 µL of MTT solution (10% MTT in PBS at 5 mg mL⁻¹ and 90% DMEM) was added, and the plates were returned to the incubator for 2 h for metabolization. After 2 h, the liquid was removed, and 100 µL of DMSO was added to elute the formazan crystals. Absorbance at 595 nm was analyzed using a spectrophotometer (Spectramax M2, Molecular Devices, USA). Absorbance was used as an index of cell viability, and the results were expressed as percentages relative to the control groups after 24 h of treatment. For greater reliability, all experiments were performed in triplicate.

5. Conclusions

We synthesized novel luminescent lanthanide complexes, specifically of europium and samarium. Subsequently, we covalently incorporated these complexes into dense or mesoporous silica nanoparticles. We then characterized these new biomarkers using various physicochemical techniques, including luminescence spectroscopy. Finally, we conducted preliminary MTT assays demonstrating robust cell viability after 24 hours of exposure to our nanoparticles in healthy cell cultures.

Supplementary Materials: The following supporting information can be downloaded at: Preprints.org.

Author Contributions: For research articles with several authors, a short paragraph specifying their individual contributions must be provided. The following statements should be used “Conceptualization, J.J. and M.A.U.M.; methodology, J.J. and S.R.S.; software, J.J., D.B. and S.R.S.; validation, J.J. and S.R.S.; formal analysis, J.J., D.B., K.F.D.P.S., S.R.S., A.P.D., M.V., R.B.A., G.R.C., A.L.P., J.R.R.A., and M.A.U.M.; investigation, J.J.; resources, J.J., D.B., K.F.D.P.S., S.R.S., A.P.D., M.V., R.B.A., G.R.C., A.L.P., J.R.R.A., and M.A.U.M.; data curation, J.J., D.B. and S.R.S.; writing—original draft preparation, J.J. writing—review and editing, J.J., A.L.P., J.R.R.A., and M.A.U.M.; visualization, M.V.; supervision, M.V. and M.A.U.M.; project administration, M.A.U.M.; funding acquisition, M.A.U.M. All authors have read and agreed to the published version of the manuscript.”

Funding: Please add: This research was funded by Universidade Federal de Mato Grosso do Sul. This study was financed in part by the Coordenação de Aperfeiçoamento de Pessoal de Nível Superior—Brasil (CAPES)—Finance Code 001 and CAPES-PrInt, Finance Code 88881.311799/2018-01. The authors are also grateful to the Conselho Nacional de Desenvolvimento Científico e Tecnológico—Brasil (CNPq)—Finance Code 420852/2018-2 and Fundação de Apoio ao Desenvolvimento do Ensino, Ciência e Tecnologia do Estado de Mato Grosso do

Sul—Brasil (FUNDECT-MS)—grants 036/2017 PPSUS-MS (59/300.074/2017) for providing financial support for undertaking this project.

Data Availability Statement: Not applicable.

Acknowledgments: The authors thanks Teófilo Fernando Mazon Cardoso for providing the FTIR analysis.

Conflicts of Interest: The authors declare no conflicts of interest.

References

1. Cousinié, S.; Mauline, L.; Gressier, M.; Kandibanda, S.R.; Datas, L.; Reber, C.; Menu, M.-J. Bulk or surface grafted silylated Ru(II) complexes on silica as luminescent nanomaterials. *New J Chem*, **2012**, 36(6), 1355-1367.
2. Li, P.; Li, H. Recent progress in the lanthanide-complexes based luminescent hybrid materials. *Coord Chem Rev*, **2021**, 441, 213988.
3. Lechevallier, S.; Jorge, J.; Silveira, R.M.; Ratel-Ramond, N.; Neumeyer, D.; Menu, M.-J.; Gressier, M.; Marçal, A.L.; Rocha, A.L.; Martines, M.A.U.; Magdeleine, E.; Dexpert-Ghys, J.; Verelst, M. Luminescence Properties of Mesoporous Silica Nanoparticles Encapsulating Different Europium Complexes: Application for Biolabelling. *J Nanomater*, **2013**, 2013, 918369.
4. Aguiar, F.P.; Costa, I.F.; Espínola, J.G.P.; Faustino, W.M.; Moura, J.L.; Brito, H.F.; Paolini, T.B.; Felinto, M.C.F.C.; Teotonio, E.E.S. Luminescent hybrid materials functionalized with lanthanide ethylenodiaminetetraacetate complexes containing β -diketonate as antenna ligands. *J Lumin* **2016**, 170, 538-546.
5. Duarte, A.P.; Gressier, M.; Menu, M.-J.; Dexpert-Ghys, J.; Caiut, J.M.A.; Ribeiro, S.J.L., Structural and Luminescence Properties of Silica-Based Hybrids Containing New Silylated-Diketonato Europium(III) Complex. *J Phys Chem C*, **2012**, 116 (1), 505-515.
6. Li, Q-P; Yan, B. Multi-walled carbon nanotube-based ternary rare earth (Eu^{3+} , Tb^{3+}) hybrid materials with organically modified silica-oxygen bridge. *J Colloid Interface Sci*, **2012**, 380, 67-74.
7. Marques, S.S.; Segundo, M.A. Nanometrics goes beyond the size: Assessment of nanoparticle concentration and encapsulation efficiency in nanocarriers. *TRAC*, **2024**, 174, 117672.
8. Narayan, R.; Nayak, U.Y.; Raichur, A.M.; Garg, S. Mesoporous Silica Nanoparticles: A Comprehensive Review on Synthesis and Recent Advances. *Pharmaceutics*, **2018**, 10(118), 1-49.
9. Léri-da-Viso, A.; Estepa-Fernández, A.; Garcia-Fernández, A.; Martí-Centelles, V.; Martínez-Máñez, R. Biosafety of mesoporous silica nanoparticles; towards clinical translation. *Adv Drug Deliv Rev*, **2023**, 201, 115549.
10. Bhatane, D.; Pamshong, S.R.; Sarnaik, S.; Prabakaran A.; Alexander, A. Potential applications of mesoporous silica nanoparticles for the treatment of neurological disorders. *J Drug Deliv Sci Technol*, **2023**, 89, 104970.
11. Jafari, S.; Derakhshankhah, H.; Alaei, L.; Fattahi, A.; Varnamkhast, B.S.; Saboury, A.A. Mesoporous silica nanoparticles for therapeutic/diagnostic applications. *Biomed Pharmacoter*, **2019**, 109, 1100-1111.
12. Abbasi, M.; Ghoran, S.H.; Niakan, M.H.; Jamali, K.; Moeini, Z.; Jangjou, A.; Izadpanah, P.; Amani, A.M. Mesoporous silica nanoparticle: Heralding a brighter future in cancer nanomedicine. *Microporous Mesoporous Mater*, **2021**, 319, 110967.
13. Zaitoun, M.A.; Momani, K.; Jaradat, Q.; Quarish, I.M. Synthesis and luminescence properties of encapsulated sol-gel glass samarium complexes. *Spectrochim Acta A Mol Biomol Spectrosc*, **2013**, 115, 810-814.
14. Choi, Y.I.; Yoon, Y.; Kang, Y.-G.; Sohn Y. Photoluminescence imaging of Eu(III) and Tb(III)-embedded SiO_2 nanostructures. *J Lumin*, **2015**, 158, 27-31.
15. Li, W.-X.; Feng, S.-Y.; Liu, Y.; Zhang, J.; Xin, X.-D.; Ao, B.-Y.; Li, Y.-J. Fluorescence enhancement of samarium (III) perchlorate by 1,10-phenanthroline on Phenyl-naphthoylmethyl sulfoxide complex and luminescence mechanism. *J Lumin*, **2013**, 143, 746-753.
16. Chen, Y.; Wu, S.; Xing, Z.; Cao, S.; Geng, X.; Yang, Y.; Xiao, L. Synthesis, structural characterization and luminescence properties of a novel europium ternary complex $\text{Eu}(2\text{-A-4-CBA})_3\text{phen}$. *J Alloys Compd*, **2015**, 649, 699-703.
17. Ćirić, A.; Stojadinović, S.; Sekulić, M.; Dramićanin, M.D. JOES: An application software for Judd-Ofelt analysis from Eu^{3+} emission spectra. *J Lumin*, **2019**, 205, 351-356.
18. Sheppard, D.A.; Maitland, C.F.; Buckley, C.E. Preliminary results of hydrogen adsorption and SAXS modelling of mesoporous silica: MCM-41. *J Alloys Compd*, **2005**, 404-406, 405-408.

19. Lunstroot, K.; Nokemann, P.; Van Hecke, K.; Van Meervelt, L.; Görrler-Walrand, C.; Binnemans, K.; Driesen, K. Visible and Near-Infrared Emission by Samarium(III) Containing Ionic Liquid Mixtures. *Inorg Chem*, **2009**, 48, 3018-3026.
20. Dyrba, M.; Miclea, P.-T.; Schweizer, S. Surface plasmons for fluorescence enhancement in Sm-doped borate glasses. *Radiat Meas*, **2010**, 45, 314-316.
21. Nehra, K.; Dalal, A.; Hooda, A.; Bhagwan, S.; Saini, R.K.; Mari, B.; Kumar, S.; Singh, D. Lanthanides β -diketonate complexes as energy-efficient emissive materials: A review. *J Mol Struct*, **2022**, 1249, 131531.
22. Bhattacharjee, S. DLS and zeta potential - What they are and what they are not? *J Control Release*, **2016**, 235, 337-351.
23. Qiao, X.-F.; Yan, B. Luminescent polymeric hybrids functionalized by β -diketone with silicon-oxygen networks and carbon chains: Assembly and characterization. *Eur Polym J*, **2009**, 45, 2002-2010.
24. He, Q.; Zhang, J.; Shi, J.; Zhu, Z.; Zhang, L.; Bu, W.; Guo, L.; Chen, Y. The effect of PEGylation of mesoporous silica nanoparticles on nonspecific binding of serum proteins and cellular responses. *Biomaterials*, **2010**, 31, 1085-1092.
25. Jorge, J; Verelst, M; Castro, GR; Martines, MAU. Effect of silica surface on luminescence properties of Tb³⁺-glutamic acid. *Int J Research Pharm Chem*, **2013**, 3(2), 184-191.
26. Zhao, XJ; Bagwe, RP; Tan, WH. Development of organic-dye-doped silica nanoparticles in a reverse microemulsion. *Adv Mater*, **2004**, 16(2), 173.
27. Mosmann, T. Rapid colorimetric assay for cellular growth and survival: application to proliferation and cytotoxicity assays. *J Immunol Methods*, **1983**, 65(1-2), 55-63.

Disclaimer/Publisher's Note: The statements, opinions and data contained in all publications are solely those of the individual author(s) and contributor(s) and not of MDPI and/or the editor(s). MDPI and/or the editor(s) disclaim responsibility for any injury to people or property resulting from any ideas, methods, instructions or products referred to in the content.